Influence of cooling rate on microstructure development of AlSi9MgMn alloy

Stanić, Davor; Zovko Brodarac, Zdenka

Source / Izvornik: **Journal of Mining and Metallurgy, Section B, Metallurgy, 2020, 56, 405 - 413**

Journal article, Published version
Rad u časopisu, Objavljena verzija rada (izdavačev PDF)

Permanent link / Trajna poveznica: https://urn.nsk.hr/urn:nbn:hr:115:995703

J. Min. Metall. Sect. B-Metall., 56 (3) (2020) 405 - 413

Journal of Mining and Metallurgy, Section B: Metallurgy

INFLUENCE OF COOLING RATE ON MICROSTRUCTURE DEVELOPMENT OF AlSi9MgMn ALLOY

D. Stanić [a,b] and Z. Zovko Brodarac [c,*]

[a] CIMOS-TCH Group P.P.C. Buzet Ltd, Buzet, Croatia
[b] Istrian University of applied sciences, Pula, Croatia
[c] University of Zagreb Faculty of Metallurgy, Sisak, Croatia

(Received 03 May 2020; accepted 03 November 2020)

Abstract

Aluminum alloys are widely applied in automotive, aircraft, food, and building industries. Multicomponent technical AlSi9MgMn alloy is primarily intended for high cooling rate technology. Controlled addition of alloying elements such as iron and manganese as well as magnesium can improve mechanical and technological properties of the final casting depending on the cooling conditions during solidification.

The aim of this investigation is the characterization of AlSi9MgMn alloy microstructure and mechanical properties at lower cooling rates than those for which this alloy was primarily developed. Thermodynamic calculation and thermal analyses revealed solidification sequence in correlation to the microstructure investigation as follows: development of primary dendrite network, precipitation of high temperature $Al_{15}(Mn,Fe)_3Si_2$ and Al_5FeSi phases, main eutectic reaction, precipitation of intermetallic $Al_8Mg_3FeSi_6$ phase, and Mg_2Si as a final solidifying phase. Influence of microstructure features investigation and cooling rate reveals significant $Al_{15}(Mn,Fe)_3Si_2$ morphology change from Chinese script morphology at low, irregular broken Chinese script morphology at medium, and globular morphology at high cooling rate. High manganese content in AlSi9MgMn alloy together with high cooling rate enables the increase of Fe+Mn total amount in the intermetallic $Al_{15}(Mn,Fe)_3Si_2$ phase and encourage favourable morphology development, all resulting in enhanced mechanical properties in as-cast state.

Keywords: *AlSi9MgMn alloy; Thermal analysis; Cooling rate; Solidification sequence; Microstructure development; Mechanical properties*

1. Introduction

Economic casting production in automotive industry implies the application of sophisticated production technologies such as high pressure die casting (HPDC) which assures achieving of good surface finish, high dimensional accuracy, and excellent mechanical properties [1,2]. Aluminium alloys have found their wide application due to enhanced microstructural, mechanical, and technological properties as a reply to high quality requirements of automotive industry [3,4]. Innovative multicomponent AlSi9MgMn (Silafont-36) is the first one with low iron and intentionally high manganese content developed for structural automotive parts production using HPDC [5].

Addition of particular alloying elements such as magnesium as well as manganese and iron can improve mechanical and technological properties of casting [6-16]. Magnesium is one of the essential alloying elements commonly added to Al–Si castings to increase their tensile strength accompanied with the degradation ductility [6-9]. Iron containing phase evolution and therefore solidification sequence of Al-Si alloys was described in detail elsewhere [6-10]. An emphasis was given on $Al_xMn_yFe_zSi_u$ phase evolution in two main manners: firstly through high temperature peritectic reaction of Al_3Fe (Al_6Mn) in liquid due to Al↔Si and later Si↔Mn position exchange in crystal lattice and secondly by independent nucleation of $Al_xMn_yFe_zSi_u$ phase [8,9]. Iron is usually considered as an inevitable impurity element in aluminum alloys and is mainly precipitated in the form of $Al_{15}(Fe,Mn)_3Si_2$ or Al_5FeSi crystals [11]. Phase Al_5FeSi is naturally hard and brittle precipitate in three-dimensional platelet form, which usually acts as a stress raiser and interferes with liquid flowing in interdendritic channels during solidification [12].

**Corresponding author: zovko@simet.unizg.hr*

https://doi.org/10.2298/JMMB200503036S

Generally, Al_5FeSi is the primary phase and the precipitation approaches the solidification onset of eutectic Al–Si when the cooling rate is increased [13,14]. Nevertheless $Al_{15}(Fe,Mn)_3Si_2$ crystals occur during eutectic solidification with α_{Al} and usually appear in polyhedral or Chinese script morphologies. The polyhedral structure forms as a primary phase [15], whereas the Chinese script structure forms at a relatively lower temperature as a coupled eutectic structure together with α_{Al} [16]. Transition elements content and there ratio have significant influence on evolution of the Al-(Mn,Fe)-Si phase [9,17], as well as cooling rate.

Understanding of the solidification mechanism of AlSi9MgMn alloy and resulting microstructure represents a challenge due to number of influenced parameters. Microstructure development is strongly dependent from chemical composition and thermodynamic conditions during solidification process [17-20]. Crystallization kinetics influence on elements interaction intensity, followed with change in intermetallics´ chemical composition and morphology. Innovative multicomponent AlSi9MgMn alloy is the first one with low iron and intentionally high manganese content. Transition elements content and there ratio have significant influence on the morphology of the Al-(Mn,Fe)-Si phase. HPDC technology favourably affect the microstructure development through evolution of intermetallic $Al_{15}(Mn,Fe)_3Si_2$ phase in globular / polyhedron manner and thus enhancing mechanical properties of castings such as ductility and toughness. Synergy of thermodynamic calculation and thermal analyses reveals solidification sequence with corresponded temperatures in correlation to microstructure investigation as follows: development of primary dendrite network, precipitation of high temperature $Al_{15}(Mn,Fe)_3Si_2$ phase, main eutectic reaction, intermetallic iron-magnesium phase precipitation $Al_8Mg_3FeSi_6$ and secondary eutectic phase $\alpha_{Al} + Mg_2Si$ as a final solidifying phase [21-28].

An impact of cooling rate during solidification process is revealed as microconstituents´ morphology, size and distribution correlated to the mechanical properties and theirs anisotropy [27-30]. Corresponding heat treatment and carefully designed regime comprehend to improved strength, better machinability of the material, increased hardness, improved dimensional stability, and eliminated residual stresses caused during casting [29,30].

Since investigated multicomponent AlSi9MgMn alloy intended for HPDC characterized with high cooling rates and therefore thin wall castings, has not been classified in European Norm (EN) [31], its solidification sequence upon different cooling condition has not been determined. The objective of this investigation is a complete characterization of the solidification behaviour of multicomponent AlSi9MgMn alloy. Therefore, the correlation of characteristic temperatures in solidification process at different cooling rates and obtained microstructure will comprehend to the estimation of applicability of this material for thick-walled safety critical parts and sets in automotive industry.

2. Experimental

Multicomponent technical AlSi9MgMn alloy is investigated using multidisciplinary approach in order to determine solidification sequence, characteristic temperature of phase transformation/precipitation and corresponding mechanical properties.

The AlSi9MgMn melt is prepared by melting of AlSi9MgMn (Silafont-36) charge material in electro-resistant furnace KONČAR-Rpa-70LX. Comparison of chemical composition of AlSi9MgMn alloy compared with commonly used AlSi9Mg alloy is shown in Table 1.

Table 1. *Chemical composition of AlSi9Mg and AlSi9Mg alloy required by norm [31,5]*

ALLOY	ELEMENT (wt. %)					
	Si	Fe	Mn	Mg	Ti	Sr
AlSi9Mg [31]	9.0 - 10.0	0.19	0.10	0.25-0.45	0.15	0.10
AlSi9MgMn [5]	9.5 - 11.5	0.15	0.50 - 0.80	0.10 - 0.50	0.04 - 0.15	0.10

Comparison of alloys reveals higher and wider range for silicon content and significantly higher manganese content in AlSi9MgMn alloy. Limitation for Fe content is stronger, while required Mn content is 5-8 times higher in AlSi9MgMn alloy when compared to common AlSi9Mg alloy. Usual ratio of Fe and Mn in similar common casting AlSi9Mg alloy corresponds to 1:0.5. In AlSi9MgMn alloy completely different ratio of Fe and Mn can be noticed. Required Mn amount is also several times higher than Fe amount in order to enhance Al-Fe,Mn-Si reaction.

After melting process, degassing was performed in order to remove captured residual hydrogen. Degassing was performed with nitrogen (N_2) using MTS-1500-FOSECO equipment with following parameters: flow Q=10 l/min, working pressure p= 0.5 MPA and degassing duration t=45 min. Gas index as a measure for process efficiency was calculated on the base of Archimedes' principle using following formula:

$$i = \left(\rho_{air} - \rho_{vacuum}\right) / \rho_{air} \cdot 100 \ [\%] \quad (1)$$

where:
ρ_{air} - density of the sample solidified in the air

ρ_{vacuum} - density of the sample solidified under the low vacuum (80 kPa).

Obtained gas index after treatment was i = 1.13% which indicate high density of an alloy after the degassing process.

Melt treatment consists of inoculation and modification with commercial master alloys in the wire form. Applied inoculant was AlTi5B1 with the target addition of 1wt.% / 1kg melt. As a modifying agent AlSr10 master alloy was added to the target content of 90 ppm of Sr.

The chemical composition of the prepared AlSi9MgMn melt was investigated using optical emission spectrometer ARL-3460 with indicated uncertainty of measurements obtained by certification with reference material.

Thermodynamic calculations of equilibrium diagram of AlSi7MgCu alloy has been performed by Thermo-Calc software TCW 5.0, with database TTAL7.

Solidification behaviour was investigated *in situ* using thermal analysis (TA) during solidification process in different moulds material and geometry in order to achieve different cooling conditions and corresponding test bars for mechanical testing. Characteristic temperatures of phase transition and precipitation were determined at different cooling rates (r_c): 0.17 °C/s, 3 °C/s, 18.7 °C/s, and 21.5 °C/s and compared with those obtained with numerical simulation by MAGMASOFT ver. 4.4 for HPDC at 63 °C/s.

Determination of characteristic temperatures for the (r_c): 0.17 °C/s was obtained using Simultaneous Thermal Analysis, Differential Scanning Calorimetry technique, with instrument STA DSC/TG, NETZSCH Jupiter 449 F1. The resolution of DSC instrument was 1µm and temperature resolution 0.001 K. Base line was determined with alumina pans. Dynamic measurements were performed in temperature interval from 25 °C to 710 °C, in argon atmosphere, with automatically controlled heating and cooling rate of 0.17 °C/s (10 °C/min). During the measurements only the energy output was followed. Measurements were repeated 2 times and the results of the second measurement were presented as referent obtained values.

Determination of characteristic temperatures for the (r_c): 3 °C/s, 12.4 °C/s, 18.7 °C/s, and 21.5 °C/s were obtained using Simple Thermal Analysis (STA) using NiCr-Ni thermocouples and NI CDAQ 9172 instrument equipped with module DAQ Pad-MI0-16XE-50 and corresponding software LabView 7.0. Casting process was performed without protective atmosphere. Measurements were repeated 2 or more times depending on the geometry of the casting and the mould material until repetitive results were obtained, which were then presented as a referent obtained values. Data acquisition was continuous

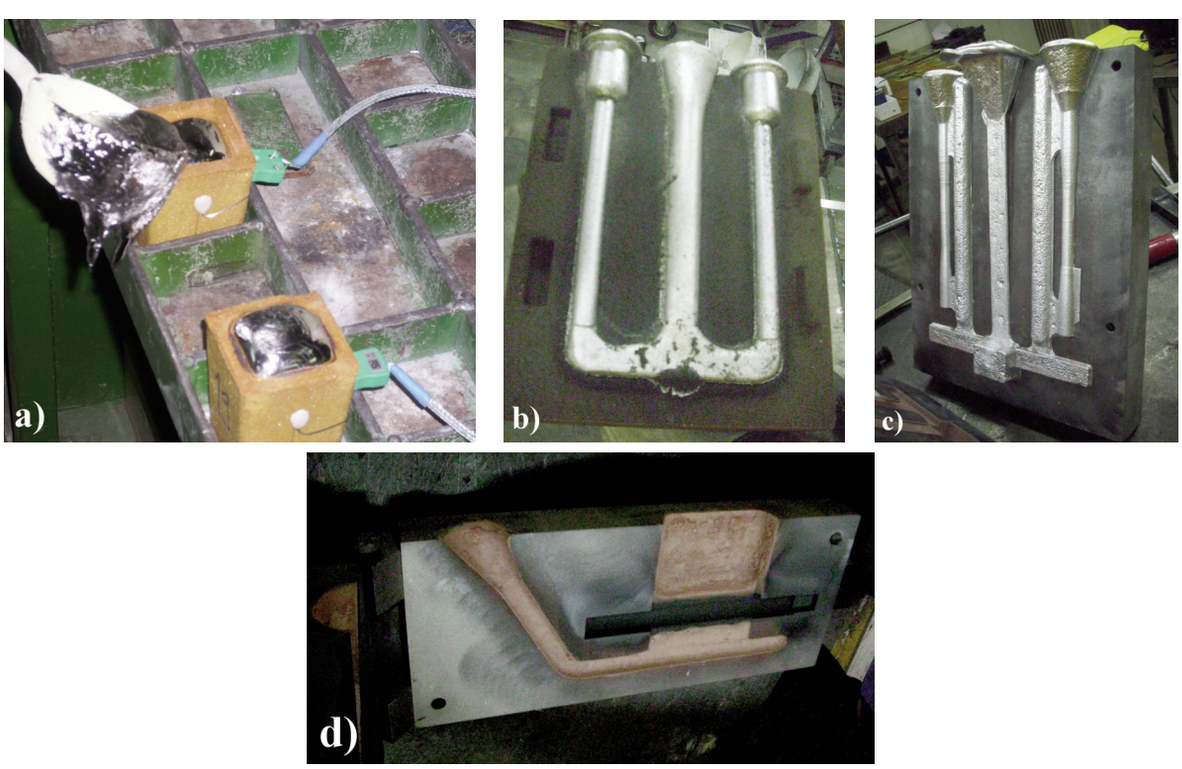

Figure 1. *Mould types used for achieving different cooling rates: a) Croning cell (3 °C/s), b) Sand mould (12.4 °C/s), c) Permanent mould - ASTM B108 mould (18.7 °C/s), d) Permanent mould (21.5 °C/s)*

during the whole solidification process starting from the pouring temperature. DAQ module and LabView software enables automatic conversion and continuous observation of the cooling curves. In order to obtain different cooling rates different mould material were used. Casting geometries were adopted in order to obtain casting shape and size which allow the production of test samples for mechanical investigation except for standard croning cell (Quick Cup equipped with NiCr-Ni thermocouple). Figure 1 shows used mould type with the indication of achieved cooling rate.

The highest cooling rate characteristic for HPDC (63 °C/s) was not measured due to limitation of the HPDC machine. Cooling curve of AlSi9MgMn in this case was calculated using MAGMASOFT ver. 4.4 software for HPDC on the base of material properties, machine parameters (melt temperature, temperatures of mould halfs, piston rates in first two casting phase, specific pressure during the third casting phase, time of mould filling, melt rate during first casting pahse, etc.) and casting geometry. Casting geometry is shown in Figure 2.

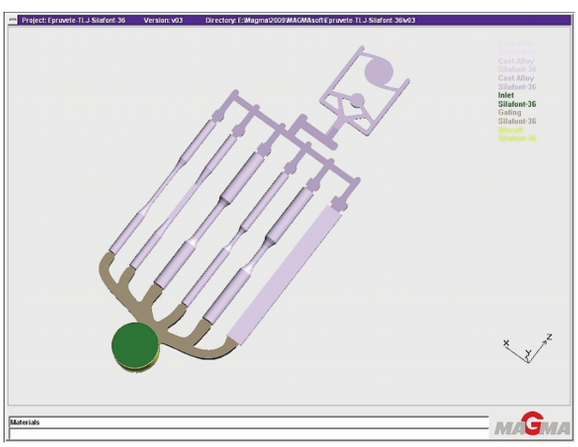

Figure 2. *Casting geometry for HPDC used for simulation with MAGMASOFT software*

Samples for metallographic investigation were taken from all castings in order to compare developed microstructures (light microscopy) and to investigate chemical composition (SEM-EDS analysis) of characteristic phases related to corresponding cooling rate. Samples were prepared by standard metallographic preparation procedure by grinding and polishing, followed by etching in 0.5% HF. Metallographic analyses cover light microscopy analysis (Olympus GX 51) and microstructural investigations using standard method at scanning electron microscope equipped with energy dispersive X-ray spectrometer (SEM-EDS, Tescan Vega TS 5136 MM). Standard SEM-EDS analysis enables mapping analysis of the characteristic region using SE detector.

Mechanical properties investigations were performed on testing machine MTS 810, at room temperature T = 20 °C in accordance to EN 10002-1:1998 [32]. Brinell hardness investigation was performed on WOLPERT DIA TESTOR 3a with sphere of 5 mm and 2500N impression force during 15 s.

3. Results and discussion

Compared overview of chemical composition of AlSi9MgMn alloy with high Mn content required by manufacturer norm [5] and real investigated sample is given in Table 2.

Comparison of chemical compositions values did not brought out any deviation from values requested by manufacturer norm [5]. Iron and manganese values significantly differ from those in common aluminium alloys, and therefore encourage formation of complex Al-(Mn,Fe)-Si phase instead of harmful Al_5FeSi phase.

Numerical modelling of equilibrium phase diagram (TCW 5.0) resulted in prediction of AlSi9MgMn alloy solidification sequence as follows in Figure 3 [22].

Dashed line indicates silicon content of 10.56 wt. % in investigated alloy. Equilibrium phase diagram indicates solidification sequence of an alloy as follows: high temperature iron/manganese phase (ALPHA#2), primary aluminium dendrite development (FCC_A1), high temperature iron and iron-manganese phase (ALPHA#1), main eutectic development (SILICON) and finally secondary eutectic phase precipitation (MG2SI). Further modelling reveals exact temperatures of phase transformations and corresponding Gibbs free energy and enthalpy. Calculated characteristic temperatures were compared with those obtained in STA DSC investigation with the lowest cooling rate (0.17 °C/s) as given in Figure 4 and Table 3.

Table 2. *Chemical composition of the AlSi9MgMn alloy [17, 19, 22, 24]*

SAMPLE	ELEMENT (wt. %)					
	Si	Fe	Mn	Mg	Ti	Sr
AlSi9MgMn [5]	9.5 -11.5	0.15	0.50 -0.80	0.10 -0.50	0.04 -0.15	0.10
AlSi9MgMn Investigated sample	10568 ± 0.15	0.0858 ± 0.019	0.6192 ± 0.009	0.2399 ± 0.009	0.0740 ± 0.0021	0.0097 ± 0.005

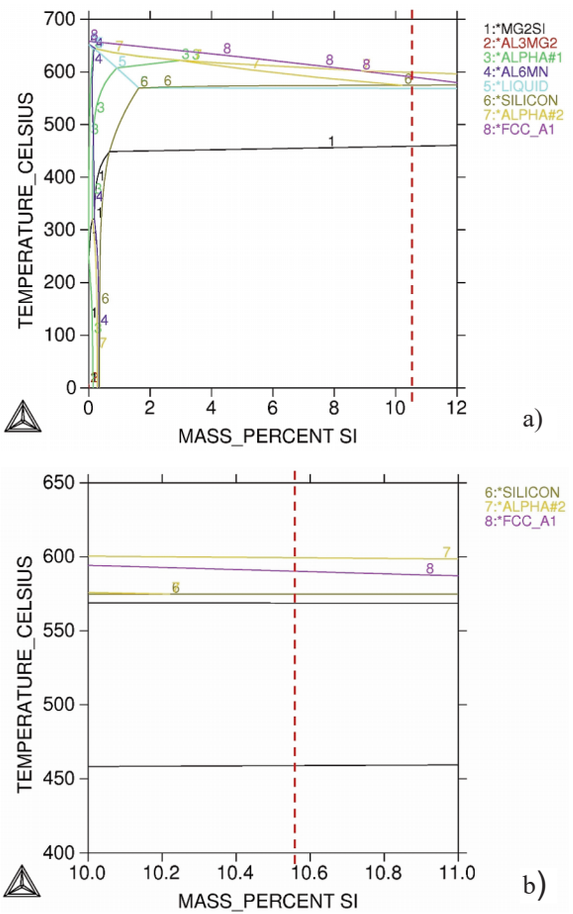

Figure 3. *Equilibrium phase diagram of investigated AlSi9MgMn alloy: a) Aluminum corner 0-12 wt.%Si, 0-700 °C, b) Aluminium corner cut 10-11 wt.%Si, 400-650 °C*

STA DSC investigation performed at controlled conditions and low cooling rate (r_c=0.17 °C/s) good coincide with TCW equilibrium temperatures except for last solidifying phase (α_{Al} + Mg_2Si) due to non-equilibrium conditions.

Simple thermal analysis was performed at cooling curves in corresponding moulds. An example of cooling curve analysis for permanent ASTM mould (18.7 °C/s) is shown in Figure 5.

Table 3. *Solidification sequence of AlSi9MgMn alloy and corresponding thermodynamic data obtained using TCW and STA DSC [22]*

No.	Reaction	ΔG x 10^4 / J/mol	ΔH x 10^4 / J/mol	T_{TCW} / °C	T_{DSC} /°C
1	$L \rightarrow L_1 + Al_3Fe$ (Al_6Mn)	-353.520	294.786	612.85	>612.0
2	$L_1 \rightarrow L_2 + \alpha_{Al}$	-336.805	285.257	589.85	588.0
3	$L_2 \rightarrow L_3 + \alpha_{Al} + Al_{15}(Mn,Fe)_3Si_2 + Al_5FeSi$	-	-	574.85	573.4
4	$L_3 \rightarrow L_4 + \alpha_{Al} + \beta_{Si}$	-325.531	229.260	573.85	571.5
5	$L_4 + Al_5FeSi \rightarrow L_5 + Al_8Mg_3FeSi_6$	-320.847	149.707	565.85	566.7
6	$L_5 \rightarrow \alpha_{Al} + Mg_2Si$	-279.466	123.504	489.85	515.7
ΔT	$\Delta T = T_2 - T_6$			100	72.3

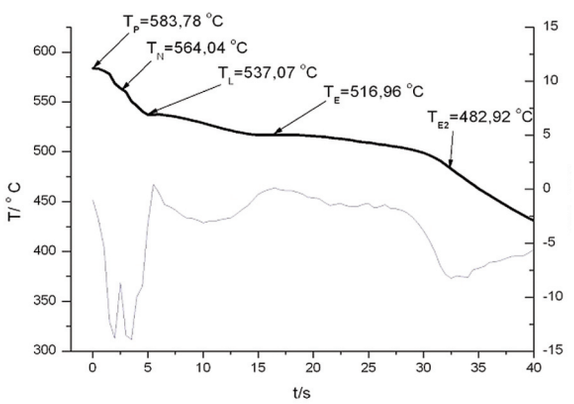

Figure 5. *Simple thermal analysis of the sample solidified with cooling rate of 18.7 °C/s*

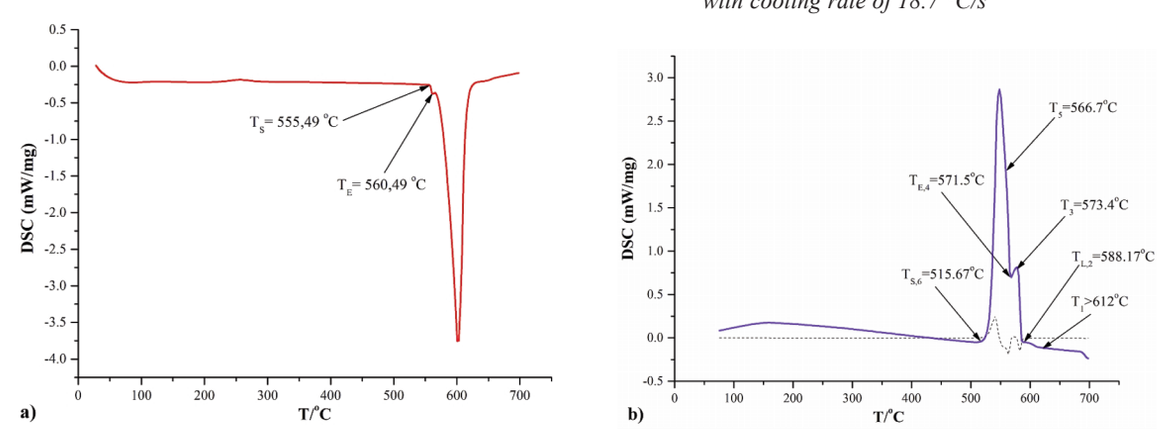

Figure 4. *STA DSC investigation of AlSi9MgMn alloy: a) heating and b) cooling curve*

Simple thermal analysis (STA) results for the cooling rates r_c: 3°C/s, 12.4 °C/s, 18.7 °C/s and 21.5 °C/s and numerical simulation using MAGMASoft (r_c=63 °C/s) are shown in Table 4.

Table 4. *Solidification sequence of AlSi9MgMn alloy and corresponding characteristic temperatures obtained using STA and MAGMASoft investigation*

No.	Reaction	r_c / °C/s				
		3	12.4	18.7	21.5	63
1	T_N: $L \rightarrow L_1 + Al_3Fe$ (Al_6Mn)	635.0	575.3	564	583.3	668.9
2	T_L: $L_1 \rightarrow L_2 + \alpha_{Al} + Al_{15}(Mn,Fe)_3Si_2 + Al_5FeSi$	579.4	531.9	537.1	534.4	606.7
3	T_E: $L_3 \rightarrow L_4 + \alpha_{Al} + \beta_{Si}$	564.1	514.1	516.9	515.1	566.9
4	T_S: $L_4 + Al_5FeSi \rightarrow L_5 + Al_8Mg_3FeSi_6 + Mg_2Si$	544.5	501.9	482.9	497.4	474.3
ΔT	$\Delta T_{L-S}=T_L-T_S$	90.5	73.4	81.1	85.9	132.4

Laboratory conditions of STA investigation, as well as different mould types, wall thickness and therefore obtained cooling rates revealed significant difference in solidification interval and characteristic temperatures´ values. The solidification temperature interval is in range from 73.4 - 90.5 °C and therefore closer to equilibrium calculation obtained by TCW. Significantly wide temperature interval has been noticed for simulated cooling rate of 63 °C/s, using MAGMASoft due to complex influenced parameters connected with HPDC technology and therefore those data are not relevant for comparison. Nucleation temperature mainly depends on the pouring temperature, so the differences in these temperatures are not of great importance for the solidification sequence process. Liquidus temperatures for low cooling rates (0.17 and 3 °C/s) achieve high values (579.4 - 588 °C), while for the medium cooling rates their values are significantly lower (531.9 - 537.1 °C). Increase of cooling rate lower the liquidus and eutectic temperature. Similar phenomenon is observed for solidus temperatures although their values are still higher than in equilibrium. In general, the increase of cooling rate in STA experiments narrows the solidification interval by lowering all the characteristic temperatures of phase transformations and intermetallic precipitation. Evolution temperature of $Al_8Mg_3FeSi_6$ phase was not identified separately from secondary Mg_2Si eutectic in any investigated case.

Microstructural investigation enables correlation of STA data with microconstituents´ appearance. The focus of investigation was pointed to the Fe-bearing phases due to different morphologies and different Mn:Fe content in correlation to cooling rate. Therefore, the appearance of characteristic microconstituents and their morphologies at three different cooling rates according to solidification interval (12.4, 18.7. and 63 °C/s) is shown in Figure 6.

Microstructural analysis using EDS enables identification of characteristic phases present in

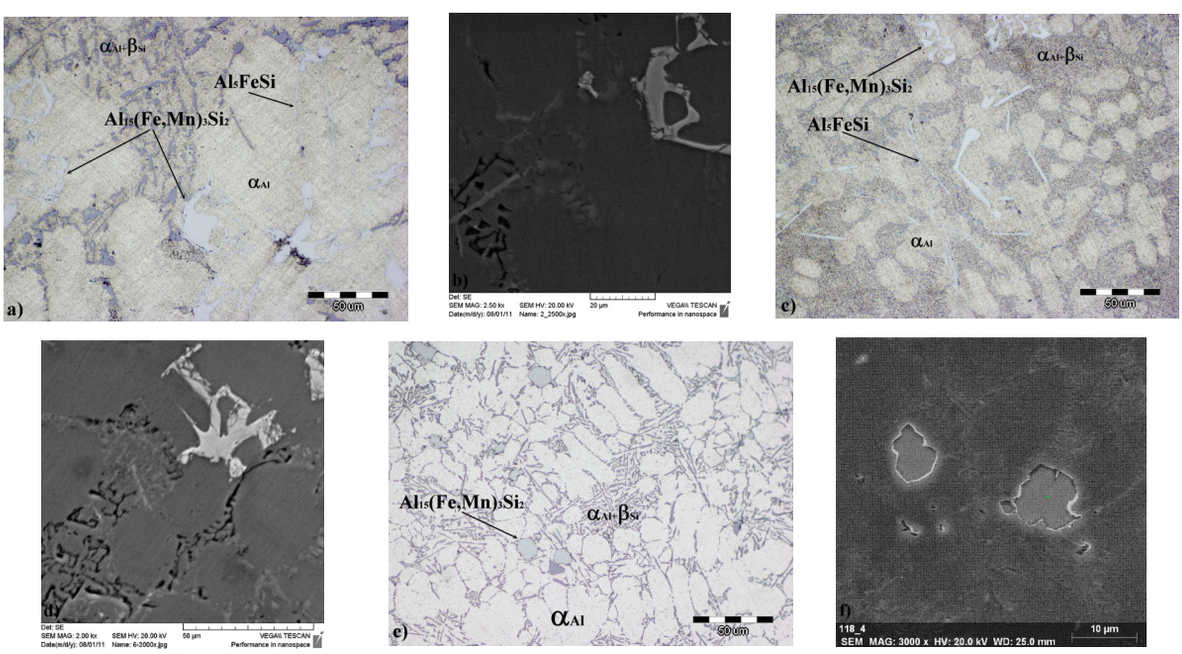

Figure 6. *Optical and SEM micrographs of the AlSi9MgMn alloy casting at different cooling rates, respectively: a) and b) 12.4 °C/s; c) and d) 18.7 °C/s, e) and f) 63 °C/s*

AlSi9MgMn alloy: primary aluminum (α_{Al}) with mixed dendrite and globular morphology, main eutectic in interdendritic spaces ($\alpha_{Al} + \beta_{Si}$). Eutectic reveals in mixed lamellar and fibrous morphology at low cooling rate (12.4 °C/s). Medium (18.7°C/s) and high (63 °C/s) cooling rates enhanced fibrous morphology of main eutectic. Iron bearing phase in AlSi9MnMg alloy develops as Al_5FeSi and $Al_{15}(Mn,Fe)_3Si_2$ in the early stage of solidification and $Al_8Mg_3FeSi_6$ together with Mg_2Si at the end of solidification. Complex intermetallic phase $Al_{15}(Mn,Fe)_3Si_2$ formed by the reaction nr. 2 (Table 4) due to both local undercooling and bulk liquid composition which allow its direct nucleation. Unfavorable needle like Al_5FeSi, magnesium bearing phase $Al_8Mg_3FeSi_6$ developed on Al_5FeSi needles and secondary eutecic phase Mg_2Si in characteristic ramified morphology distributed at the grain boundaries were detected at lower cooling rates (12.4, 18.7 °C/s).

Typical Fe bearing phase in AlSi9MnMg alloy develops as a Al_5FeSi and $Al_{15}(Mn,Fe)_3Si_2$. Even at low cooling rates high Mn content favours development of independently precipitated $Al_{15}(Mn,Fe)_3Si_2$ phase. Increase of cooling rate comprehend to transformation of $Al_{15}(Mn,Fe)_3Si_2$ phase morphology from coarse broken Chinese script at low cooling rate, across regular Chinese script morphology at medium one to polyhedron morphology at high cooling rate. Microstructure investigation included analysis of Fe and Mn atomic ratio in different morphologies, as shown in Table 5.

Performed microstructural investigations indicate

Table 5. *Atomic ratio of $Al_{15}(Mn,Fe)_3Si$ phase constituent*

r_c / °C/s	Al	Mn	Fe	Si	Mn:Fe	Mn+Fe
	at.%					
12.4	72.48	14.87	2.54	10.12	5.86	17.41
18.7	72.50	14.75	2.48	10.29	5.95	17.23
63	72.83	15.05	2.75	9.37	5.47	17.80
Average	72.60	14.89	2.59	9.92	5.76	17.48

significant differences in morphology and relationship between Mn and Fe as variable constituents of $Al_{15}(Mn,Fe)_3Si_2$ phase in dependence from cooling rate, as shown in Figure 7.

Increase of cooling rate generally promotes the increase of total amount of (Mn+Fe) due to the independent nucleation of $Al_{15}(Mn,Fe)_3Si_2$ phase from Chinese script to globular manner. Low cooling rate (12.4 °C) microstructure consists from both Fe-bearing phases $Al_{15}(Mn,Fe)_3Si_2$ and Al_5FeSi, which explains predominant role of Fe in intermetallics development. Medium cooling rate (18.7 °C) reveals higher impact of Mn in preferably formation of $Al_{15}(Mn,Fe)_3Si_2$ phase resulting with the highest

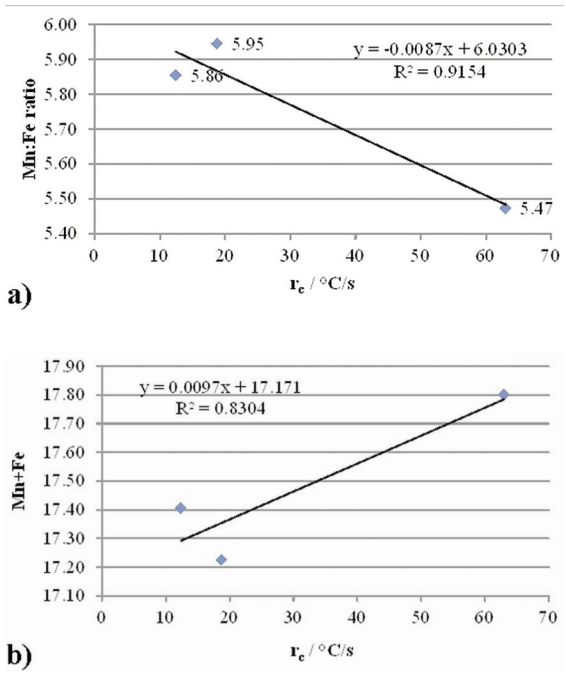

Figure 7. *Influence of cooling rate on $Al_{15}(Mn,Fe)_3Si_2$ phases morphology development: a) (Mn:Fe) ratio and b) Mn+Fe values*

Mn:Fe ratio and smallest total (Fe+Mn) content. The highest cooling rate (63°C/s) does not allow significant replacement of Mn and Fe atoms in crystal lattice which results in smallest Mn:Fe ratio and highest total (Fe+Mn) content due to independent nucleation of $Al_{15}(Mn,Fe)_3Si_2$ phase.

Mechanical properties' values were compared for typical cooling rates, as indicated in Table 6.

Table 6. *Comparison of mechanical properties in dependence to different cooling rates*

r_c / °C/s	$\Delta T_{L-S}=T_L-T_S$ / °C	$R_{p0,2}$ / N/mm²	R_m / N/mm²	Δl / %	HB
12.4	90.5	102	165	1.8	73.8
18.7	81.1	110	204	2.5	76.3
63	132.4	153	306	5.8	85.2

The best mechanical properties were displayed by samples solidified at highest cooling rate (63 °C/s) typical for HPDC. Low cooling rates resulted in weaker mechanical properties due to unfavourable microstructure features of main eutectic and Fe-bearing phases. The only microstructural constituent which significantly changes its' morphology and size was $Al_{15}(Mn,Fe)_3Si_2$. Widening the solidification interval favours transition from needle like Al_5FeSi across ramified Chinese script to globular $Al_{15}(Mn,Fe)_3Si_2$ morphology due to increase of total (Mn+Fe) ratio and also lowering the Mn:Fe ratio. Although, investigated AlSi9MnMg alloy was

developed for HPDC and obtained mechanical properties are in line with requirement for complex castings produced with other technologies with lower cooling rates (sand casting, gravity die casting). Brinell hardness (HB) did not reveal significant deviations relating to particular cooling rates, which indicates that matrix hardness is the most influential on overall hardness. Reduced HB for lower cooling rates (for ~10HB) can be correlated to shorter solidification interval for solid solution development. Obtained HB values are in line with requirement for investigated alloy [5].

4. Conclusions

Multicomponent technical AlSi9MgMn alloy with high manganese content developed for high pressure die casting (HPDC) was investigated in this work at lower cooling rate conditions in order to indicate the application potential through characterization of microstructure development and obtained mechanical properties. Applied cooling rates (3, 12.4 °C/s, 18.7 °C/s, 21.5 °C/s and 63 °C/s) influence on change of thermodynamic, microstructural and mechanical properties of AlSi9MgMn alloy. Characterization of AlSi9MgMn behavior at lower cooling rates than those for which it has been developed (HPDC) reveals following conclusions:

• Significant temperatures of phase transformation (liquidus and eutectic temperature) are lower while solidus temperature is higher than those for equilibrium solidification.

• Lower cooling rates narrow solidification interval when compared to equilibrium and simulated values.

• Microstructure development indicates Fe-bearing microconstituents with different morphology relating to cooling rate. Solidification starts with primary dendrite network (α_{Al}) and both $Al_{15}(Mn,Fe)_3Si_2$ (Chinese script at medium and polyhedron at high cooling rates) + Al_5FeSi (needle like at low cooling rate) phases development, followed with main eutectic ($\alpha_{Al} + \beta_{Si}$) transformation and finally ended with Mg-intermetallics such as $Al_8Mg_3FeSi_6$ and Mg_2Si.

• Increase of cooling rates and high manganese content encourage transformation of Fe-bearing phase from needle like Al_5FeSi toward coarse broken Chinese script at low cooling rate, across regular Chinese script morphology at medium to polyhedron morphology at high cooling rate in corresponding $Al_{15}(Mn,Fe)_3Si_2$ stoichiometry.

• High manganese content influences on Mn-Fe ratio change in $Al_{15}(Mn,Fe)_3Si_2$ phase. Increase of cooling rate influence on decrease of Mn:Fe ratio and increase on total Mn+Fe amount in investigated phases'.

• Increase of cooling rate acts favourably to increase of yield and tensile strength, elongation and Brinell hardness due to change of microconstituent's morphology.

Although the target medium cooling rate indicates the highest Mn:Fe ratio and the lowest Mn+Fe value resulting in regular Chinese script morphology of Fe-bearing phase, obtained strength and hardness reveal high values in as-cast state. Determination of differences in microstructure development during solidification process and the characterization of thermodynamic, microstructural, and mechanical properties of multicomponent AlSi9MgMn alloy at low and medium cooling rate conditions comprehends to evaluation of overall applicability of this material for thick-walled safety critical parts and sets in automotive industry solidified at lower cooling rate.

Acknowledgements

Investigations have been performed in collaboration with company CIMOS-P.P.C. Buzet, d.o.o., Buzet, Croatia. Investigations were performed within the Institutional project IP-124 funded by University of Zagreb Faculty of Metallurgy, topic "Design and Characterization of Innovative Engineering Alloys", Infrastructural scientific project: Centre for Foundry Technology - SIMET, KK.01.1.1.02.0020 funded by European Regional Development Fund, Operational Programme Competitiveness and Cohesion 2014 - 2020. and Infrastructural scientific project: VIRTULAB - Integrated laboratory for primary and secondary raw materials, KK.01.1.1.02.0022 funded by European Regional Development Fund, Operational Programme Competitiveness and Cohesion 2014 - 2020.

References

[1] F. Bonollo, N. Gramegna, G. Timelli, JOM, 67 (5) (2015) 901–908.

[2] F. Casarotto, A. J. Franke, R. Franke, in Advanced Materials in Automotive Engineering (J. Rowe), Woodhead Publishing Limited, Cambridge, UK, 2012, p. 109-149.

[3] Z.Z. Brodarac, D. Stanić, Proceedings book of MATRIB 2014, Croatian Society for materials and tribology, June, 26-28, Vela Luka, Croatia, 2014, p. 637-646.

[4] N. Dolić, Z.Z. Brodarac, J. Min. Metall. Sect. B-Metall., 53 (3) (2017) 429 – 439.

[5] RHEINFELDEN, catalogue: SILAFONT 36 - AlSi9MgMn.

[6] G. Barlock, L. F. Mondolfo, Z .Metallkd., 66 (10) (1995) 605-611.

[7] J. E. Tibballs, J. A. Horst, C. J. Simensen, J. Mater. Sci., 36 (4) (2001) 937-941.

[8] M. Warmuzek, K. Rabczak, J. Sieniawski, J. Mater.

Process Tech., 162–163 (2005) 422–428.
[9] M. Warmuzek, J. Sieniawski, K. Wicher, G. Mrówka, J. Mater. Process Tech., 175 (1-3) (2006) 421–426.
[10] L. Backerund, G. Chai, J. Tamminen, Solidification Characteristics of Aluminium Alloys, Volume 2, Foundry Alloys, AFS/Skanaluminium, Stockhlom, Sweden, 1999.
[11] M. V. Kral, Mater. Lett., 59 (18) (2005) 2271–2276.
[12] M. Tash, F. H. Samuel, F. Mucciardi, Mat. Sci. Eng. A-Struct., 443 (1-2) (2007), 185–201.
[13] S. Belmares-Perales, M. Castro-Román, M. Herrera-Trejo, L. E. Ramírez-Vidaurri, Met. Mater. Int., 14 (3) (2008) 307-314.
[14] A. Couture, Int. Cast. Met. J., 6 (4) (1981) 9-17.
[15] P. N. Crepeau, AFS Transactions, 103 (1995) 361-366.
[16] C. M. Dinnis, J. A. Taylor, A. K. Dahle, Scripta Mater., 53 (8) (2005) 955–958.
[17] Z.Z. Brodarac, D. Stanić, 71st World Foundry Congress: Advanced Sustainable Foundry; World Foundry Organization, May, 19-21, Bilbao, Spain, 2014, p.1223-1227.
[18] U. Büyük, S. Engin, N. Maraşli, J. Min. Metall. Sect. B- Metall., 51 (1) (2015) 67 - 72.
[19] Z.Z. Brodarac, N. Dolić, F. Unkić, J. Min. Metall. Sect. B- Metall., 50 (1) (2014) 53-60.
[20] Z.Z. Brodarac, F. Unkić, J. Medved, P. Mrvar, Kovove Mater., 50 (1) (2012) 59–67.
[21] Z.Z. Brodarac, T. Holjevac Grgurić, J. Burja, J. Therm Anal. Calorim. 127 (2017) 431–438
[22] Z.Z. Brodarac, D. Stanić, F. Unkić, Livarski vestnik, 60 (4) (2013) 201-215.
[23] R. Liu, J. Zheng, L. Godlewski, J. Zindel, M. Li, W. Li, S. Huang, Mat .Sci. Eng.A-Struct., 783 (2020) 139280.
[24] Z.Z. Brodarac, D. Stanić, Livarski vestnik, 62 (4) (2015) 195-208.
[25] Q. Cai, C. L. Mendis, I.T.H. Chang, Z. Fan, Mater. Des., 187 (2020) 108394.
[26] M. Vončina, J. Medved, S. Kores, P. Xiec, P. Schumacher, J. Li, Mater. Charact., 155 (2019) 109820.
[27] Z.Z. Brodarac, P. Mrvar, J. Medved, P. Fajfar, Metalurgija, 46 (1) (2007) 29-35.
[28] Z.Z. Brodarac, D. Stanić, Book of Abstracts of the 5th Central and Eastern Conference on Thermal Analysis and Calorimetry (CEEC-TAC5) and 14th Mediterranean Conference on Calorimetry and Thermal Analysis (Medicta2019), Central and Eastern Commitee on Thermal Analysis and Calorimetry, August, 27-30, Roma, Italy, 2019, p.143.
[29] M. Vončina, S. Kores, M. Ernecl, J. Medved, J. Min. Metall. Sect. B- Metall., 53 (3) (2017) 423 – 428.
[30] B. Jordović, B. Nedeljković, N. Mitrović, J. Živanić, A. Maričić, J. Min. Metall. Sect. B- Metall., 50 (2) (2014) 133 – 137.
[31] EN 1706:2010 Aluminium and aluminium alloys - Castings - Chemical composition and mechanical properties.
[32] EN 10002-1:1998 Metallic materials – Tensile testing – Part 1: Method of test (at ambient temperature).

UTICAJ BRZINE HLAĐENJA NA RAZVOJ MIKROSTRUKTURE AlSi9MgMn LEGURE

D. Stanić [a,b] and Z. Zovko Brodarac [c,*]

[a] CIMOS-TCH Grupa P.P.C. Buzet Ltd, Buzet, Hrvatska
[b] Politehnika Pula–fakultet za primenjene nauke, Pula, Hrvatska
[c] Univerzitet u Zagrebu Metalurški fakultet, Sisak, Hrvatska

Apstrakt

Legure aluminijuma imaju široku primenu u automobilskoj, avionskoj, prehrambenoj i građevinskoj industriji. Višekomponentna tehnička AlSi9MgMn legura ima primarnu namenu u tehnologiji brzog hlađenja. Kontrolisano dodavanje legirajućih elemenata kao što su železo i mangan, kao i magnezijuma, može poboljšati mehaničke i tehnološke osobine završnog livenja u zavisnosti od uslova hlađenja tokom solidifikacije.

Cilj ovog istraživanja je karakterizacija mikrostrukture AlSi9MgMn legure i mehaničkih osobina pri nižim brzinama hlađenja od onih za koje je ova legura primarno namenjena. Termodinamički proračuni i termalna analiza otkrili su redosled solidifikacije u odnosu na istraživanje mikrostrukture, i to na ovaj način: razvoj primarne dendritne mreže, precipitacija visokotemperaturnih $Al_{15}(Mn,Fe)_3Si_2$ i Al_5FeSi faza, glavna eutektička reakcija, precipitacija intermetalične $Al_8Mg_3FeSi_6$ faze, i Mg_2Si kao finalna faza solidifikacije. Istraživanje uticaja mikrostrukturnih osobina i brzine hlađenja otkriva značajnu morfološku promenu $Al_{15}(Mn,Fe)_3Si_2$ od morfologije kineskog pisma pri niskim, nepravilne morfologije kineskog pisma pri srednjim, i globularne morfologije pri visokim brzinama hlađenja. Visok sadržaj mangana u AlSi9MgMn leguri zajedno sa visokom brzinom hlađenja omogućava povećanje ukupne količine Fe+Mn u intermetaličnoj $Al_{15}(Mn,Fe)_3Si_2$ fazi i podstiče povoljan morfološki razvoj, što sve rezultira poboljšanim mehaničkim osobinama u izlivenom stanju.

Ključne reči: *AlSi9MgMn legura; Termalna analiza; Brzina hlađenja; Redosled solidifikacije; Razvoj mikrostrukture; Mehaničke osobine*